KSCE Journal of Civil Engineering (2011) 15(8):1405-1414
DOI 10.1007/s12205-011-1361-z

Structural Engineering

www.springer.com/12205

A New Trigonometric Shear Deformation Theory for Bending Analysis of Functionally Graded Plates Resting on Elastic Foundations

Mohammed Ameur*, Abdelouahed Tounsi, Ismail Mechab***, and El Abbes Adda Bedia******

Received October 21, 2010/Revised December 21, 2010/Accepted February 17, 2011

Abstract

A new trigonometric shear deformation plate theory involving only four unknown functions, as against five functions in case of other shear deformation theories, is developed for flexural analysis of Functionally Graded Material (FGM) plates resting on an elastic foundation. The theory presented is variationally consistent, has strong similarity with classical plate theory in many aspects, does not require shear correction factor, and gives rise to transverse shear stress variation such that the transverse shear stresses vary parabolically across the thickness satisfying shear stress free surface conditions. In the analysis, the two-parameter Pasternak and Winkler foundations are considered. Material properties of the plate are assumed to be graded in the thickness direction according to a simple power-law distribution in terms of the volume fractions of the constituents. Governing equations are derived from the principle of virtual displacements. The accuracy of the present theory is demonstrated by comparing the results with solutions derived from other higher-order models found in the literature. It can be concluded that the proposed theory is accurate and simple in solving the static bending behavior of functionally graded plates.

Keywords: *functionally graded plates, shear deformation theory, higher-order theory, Navier solution*

1. Introduction

Plates supported by elastic foundations have been widely adopted by many researchers to model various engineering problems during the past decades. Such plate structures can be found in various kinds of industrial applications like raft foundations, storage tanks, swimming pools, and in most civil engineering constructions. One- and two-parameter models for the soil underneath the plate are introduced to model the foundation. The Pasternak model (Pasternak, 1954) or the two-parameter model is widely adopted to describe the mechanical behavior of foundations, and the well known Winkler model (Winkler, 1867) is one of its special cases. In fact, the two-parameter elastic foundation models have been developed to overcome the inadequacy of Winkler model in describing the real soil response and the mathematical complexity of the three-dimensional continuum. The two-parameter model (Pasternak model) considers the shear deformation between the springs over the one-parameter model whilst the one-parameter model (Winkler model) can be represented by continuous springs. Therefore, Winkler model can be considered as a special case of Pasternak model by setting the shear modulus to zero.

On the other hand, Functionally Graded Materials (FGMs) (Koizumi, 1993; Suresh and Mortensen, 1998), a new generation of advanced inhomogeneous composite materials first proposed for thermal barriers (Koizumi, 1997), have been increasingly applied for modern engineering structures in extremely higher temperature environment. Many researches were conducted concerning thermal mechanical behavior of FGMs (Tanigawa, 1995; Suresh and Mortensen, 1997). However, bending and vibration analyses of FGMs are quite limited, especially of those on elastic foundations. Cheng and Kitipornchai (1999) proposed a membrane analogy to derive an exact explicit eigenvalues for compression buckling, hydrothermal buckling, and vibration of FGM plates on a Winkler-Pasternak foundation based on the first-order shear deformation theory. The same membrane analogy was later applied to the analyses of FGM plates and shells based on a third-order plate theory (Cheng and Batra, 2000; Reddy and Cheng, 2002). Recently, Ait Atmane *et al.* (2010) developed a new higher shear deformation theory to investigate the free vibration analysis of simply supported functionally graded plates resting on a Winkler-Pasternak elastic foundation.

This paper aims to provide a new trigonometric shear deformation plate theory for the bending behavior of FGM thick plates

*Doctor, Université Ibn Khaldoun, 14000 Tiaret, Algérie (E-mail: mohammed.ameur@gmail.com)
**Professor, Laboratoire des Matériaux & Hydrologie, Université de Sidi Bel Abbes, 22000 Sidi Bel Abbes, Algérie (Corresponding Author, E-mail: tou_abdel@yahoo.com)
***Doctor, Laboratoire des Matériaux & Hydrologie, Université de Sidi Bel Abbes, 22000 Sidi Bel Abbes, Algérie (E-mail: ismyala@yahoo.fr)
****Professor, Laboratoire des Matériaux & Hydrologie, Université de Sidi Bel Abbes, 22000 Sidi Bel Abbes, Algérie (E-mail: addabed@yahoo.com)

on a Winkler-Pasternak foundation. The present trigonometric plate theory contains only four unknown functions, as against five functions in the case of the well- known Reddy's Parabolic Shear Deformation Plate Theory (PSDPT) (Reddy, 1984), Touratier's Sinusoidal Shear Deformation Plate Theory (SSDPT) (Touratier, 1991), Karama's Exponential Shear Deformation Plate Theory (ESDPT) (Karama *et al.*, 2003) and the First Shear Deformation Plate Theory (FSDPT), but results in more accurate prediction of deflections and stresses, and satisfy the zero tangential traction boundary conditions on the surfaces of the plate. However, the present theory and other Higher-order Plate Theories (HPT) do not require the use of shear correction factors. In conclusion, the present theory gives more accurate results, especially transverse shear stresses, than other Higher-order Plate Theories (HPT).

2. Problem Formulation

Consider a solid rectangular plate of length a, width b and thickness h made of functionally graded material with the coordinate system as shown in Fig. 1. It is assumed to be rested on a Winkler-Pasternak type elastic foundation with the Winkler stiffness of $\boldsymbol{k}_0$ and shear stiffness of $\boldsymbol{k}_1$. The material properties of the FGM plate, such as Young's modulus $\boldsymbol{E}$ is assumed to be function of the volume fraction of constituent materials. Let the FGM plate be subjected to a transverse load $\boldsymbol{q}(\boldsymbol{x}, \boldsymbol{y})$.

The rectangular Cartesian plan form co-ordinates $\boldsymbol{x}$ and $\boldsymbol{y}$ are introduced in the deformation analysis of the present plate. The considered plate is bounded by the co-ordinate planes $\boldsymbol{x} = 0$, $\boldsymbol{a}$ and $\boldsymbol{y} = 0$, $\boldsymbol{b}$. The reference surface is the middle surface of the plate defined by $\boldsymbol{z} = 0$, and $\boldsymbol{z}$ denotes the thickness co-ordinate measured from the un-deformed middle surface.

Two homogenization techniques are used to find the effective properties at each point in FGM layer. The rule of mixtures is the conventional and simple technique which is widely used in composite materials. In this technique, the effective property of FGM can be approximated based on an assumption that a composite property is the volume weighted average of the properties of the constituents. Another widely used approach for characterization of the material gradation is the micromechanics technique. In this technique, the effective elastic moduli of an FGM are determined from the volume fractions and shapes of the constituents. The Mori-Tanaka method (Mori and Tanaka, 1973) and self-consistent method (Hill, 1965) are two popular schemes of micromechanics technique. Recently, Chehel Amirani *et al.* (2009) studied the free vibration of sandwich beam with FG core and they showed that there is insignificant difference between the results obtained by these two techniques (micromechanics technique and the rule of mixtures technique). Hence, in the following sections, the rule of mixtures technique is used for its simplicity.

The functional relationship between $\boldsymbol{E}$ and $\boldsymbol{z}$ for the ceramic and metal FGM plate is assumed as (Ait Atmane, 2010; Praveen and Reddy, 1998; Mechab *et al.*, 2010)

$$\boldsymbol{E}(\boldsymbol{z}) = \boldsymbol{E}_{\boldsymbol{m}} + \boldsymbol{E}_{\boldsymbol{cm}} \boldsymbol{V}_{\boldsymbol{f}} \tag{1a}$$

Where

$$\boldsymbol{E}_{\boldsymbol{cm}} = \boldsymbol{E}_{\boldsymbol{c}} - \boldsymbol{E}_{\boldsymbol{m}}\,,\ \boldsymbol{V}_{\boldsymbol{f}} = \left(\frac{1}{2} + \frac{\boldsymbol{z}}{\boldsymbol{h}}\right)^{\boldsymbol{p}} \tag{1b}$$

where $\boldsymbol{E}_{\boldsymbol{c}}$ and $\boldsymbol{E}_{\boldsymbol{m}}$ are the corresponding properties of the ceramic and metal, respectively, and $\boldsymbol{p}$ is the volume fraction exponent which takes values grater than or equal to zero. The above power-law assumption reflects a simple rule of mixtures used to obtain the effective properties of the ceramic–metal plate. The rule of mixtures applies only to the thickness direction. Note that the volume fraction of the metal is high near the bottom surface of the plate, and that of ceramic high near the top surface. In addition, (1) indicates that the bottom surface of the plate ($\boldsymbol{z} = -\boldsymbol{h}/2$) is metal-rich whereas the top surface ($\boldsymbol{z} = \boldsymbol{h}/2$) of the plate is ceramic-rich. Generally, Poisson's ratio $\boldsymbol{v}$ varies in a small range. For simplicity, $\boldsymbol{v}$ is assumed constant across the plate thickness. Fig. 2 shows the volume fraction distribution of metallic phase through the thickness for several values of the power law index. The value of $\boldsymbol{p}$ equal to zero represents a fully ceramic plate and infinite $\boldsymbol{p}$ a fully metallic plate. The variation of the composition of ceramics and metal is linear for $\boldsymbol{p} = 1$. When the value of $\boldsymbol{p}$

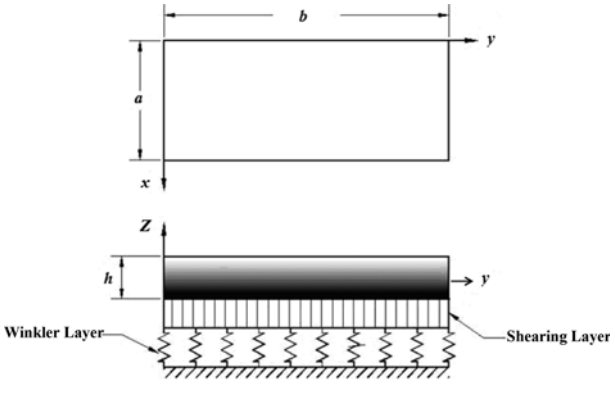

Fig. 1. FGM Plate Resting on Elastic Foundation

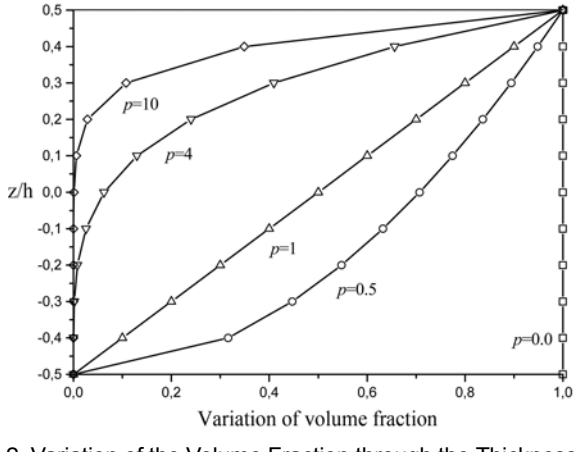

Fig. 2. Variation of the Volume Fraction through the Thickness of a Plate

increases or the volume fraction V_f decreases, the content of metal in an FG plate increases.

2.1 Higher-order Plate Theory:

The displacements of a material point located at (x, y, z) in the plate may be written as:

$$u = u_0(x,y) - z\frac{\partial w_0}{\partial x} + \Psi(z)\theta_x \tag{2a}$$

$$v = v_0(x,y) - z\frac{\partial w_0}{\partial y} + \Psi(z)\theta_y \tag{2b}$$

$$w = w_0(x,y) \tag{2c}$$

where, u, v, w are displacements in the x, y, z directions, u_0, v_0 and w_0 are midplane displacements, θ_x and θ_y rotations of the yz and xz planes due to bending, respectively. $\Psi(z)$ represents shape function determining the distribution of the transverse shear strains and stresses along the thickness. The displacement field of the Classical thin Plate Theory (CPT) is obtained easily by setting $\Psi(z) = 0$. The displacement of the First-order Shear Deformation Plate Theory (FSDPT) is obtained by setting $\Psi(z) = z$. Also, the displacement of Third-order Shear Deformation Plate Theory (TSDPT) of Reddy (1984) is obtained by setting:

$$\Psi(z) = z\left(1 - \frac{4z^2}{3h^2}\right) \tag{3a}$$

The sinusoidal shear deformation plate theory (SSDPT) of Touratier (1991) is obtained by setting:

$$\Psi(z) = \frac{h}{\pi}\sin\left(\frac{\pi z}{h}\right) \tag{3b}$$

In addition, the Exponential Shear Deformation Plate Theory (ESDPT) of Karama *et al.* (2003) is obtained by setting:

$$\Psi(z) = ze^{-2(z/h)^2} \tag{3c}$$

2.2 Present Refined Hyperbolic Shear Deformation Theory

Unlike the other theories, the number of unknown functions involved in the present Refined Hyperbolic Shear Deformation Theory (RHSDT) is only four, as against five in case of other shear deformation theories (Reddy, 1984; Touratier, 1991; Karama *et al.*, 2003). The theory presented is variationally consistent, does not require shear correction factor, and gives rise to transverse shear stress variation such that the transverse shear stresses vary parabolically across the thickness satisfying shear stress free surface conditions.

2.2.1 Assumptions of the Present Plate Theory (RHSDT)

Assumptions of the (RHSDT) are as follows:

1. The displacements are small in comparison with the plate thickness and, therefore, strains involved are infinitesimal.
2. The transverse displacement w includes two components of bending w_b, and shear w_s. These components are functions of coordinates x, y only.

$$w(x,y,z) = w_b(x,y) + w_s(x,y) \tag{4}$$

3. The transverse normal stress σ_z is negligible in comparison with in-plane stresses σ_x and σ_y.
4. The displacements u in x-direction and v in y-direction consist of extension, bending, and shear components.

$$U = u_0 + u_b + u_s\,,\ V = v_0 + v_b + v_s \tag{5}$$

The bending components u_b and v_b are assumed to be similar to the displacements given by the classical plate theory. Therefore, the expression for u_b and v_b can be given as:

$$u_b = -z\frac{\partial w_b}{\partial x}\,,\ v_b = -z\frac{\partial w_b}{\partial y} \tag{6}$$

The shear components u_s and v_s give rise, in conjunction with w_s, to the parabolic variations of shear strains γ_{xz}, γ_{yz} and hence to shear stresses τ_{xz}, τ_{yz} through the thickness of the plate in such a way that shear stresses τ_{xz}, τ_{yz} are zero at the top and bottom faces of the plate. Consequently, the expression for u_s and v_s can be given as:

$$u_s = -f(z)\frac{\partial w_s}{\partial x}\,,\ v_s = -f(z)\frac{\partial w_s}{\partial y} \tag{7}$$

2.2.2 Kinematics and Constitutive Equations

Based on the assumptions made in the preceding section, the displacement field can be obtained using Eqs. (4)-(7) as:

$$u(x,y,z) = u_0(x,y) - z\frac{\partial w_b}{\partial x} - f(z)\frac{\partial w_s}{\partial x}$$

$$v(x,y,z) = v_0(x,y) - z\frac{\partial w_b}{\partial y} - f(z)\frac{\partial w_s}{\partial y}$$

$$w(x,y,z) = w_b(x,y) + w_s(x,y) \tag{8a}$$

where

$$f(z) = z - \frac{h}{\pi}\sin\left(\frac{\pi z}{h}\right) \tag{8b}$$

The strains associated with the displacements in Eq. (8) are:

$$\varepsilon_x = \varepsilon_x^0 + zk_x^b + f(z)k_x^s$$

$$\varepsilon_y = \varepsilon_y^0 + zk_y^b + f(z)k_y^s$$

$$\gamma_{xy} = \gamma_{xy}^0 + zk_{xy}^b + f(z)k_{xy}^s$$

$$\gamma_{yz} = g(z)\gamma_{yz}^s$$

$$\gamma_{xz} = g(z)\gamma_{xz}^s$$

$$\varepsilon_z = 0 \tag{9}$$

where

$$\varepsilon_x^0 = \frac{\partial u_0}{\partial x}\,,\ k_x^b = \frac{\partial^2 w_b}{\partial x^2}\,,\ k_x^s = -\frac{\partial^2 w_s}{\partial x^2}$$

$$\varepsilon_y^0 = \frac{\partial u_0}{\partial y}\,,\ k_y^b = \frac{\partial^2 w_b}{\partial y^2}\,,\ k_y^s = -\frac{\partial^2 w_s}{\partial y^2}$$

$$\gamma_{xy}^0 = \frac{\partial u_0}{\partial y} + \frac{\partial v_0}{\partial x}\,,\ k_{xy}^b = -2\frac{\partial^2 w_b}{\partial x \partial y}\,,\ k_{xy}^s = -2\frac{\partial^2 w_s}{\partial x \partial y}$$

$$\gamma_{yz}^{s}=\frac{\partial w_s}{\partial y},\ \gamma_{xz}^{s}=\frac{\partial w_s}{\partial x},\ g(z)=1-f'(z)\ \text{and}\ f'(z)=\frac{df(z)}{dz} \tag{10}$$

For elastic and isotropic FGMs, the constitutive relations can be written as:

$$\begin{Bmatrix}\sigma_x\\ \sigma_y\\ \tau_{xy}\end{Bmatrix}=\begin{bmatrix}Q_{11}&Q_{12}&0\\ Q_{12}&Q_{22}&0\\ 0&0&Q_{66}\end{bmatrix}\begin{Bmatrix}\varepsilon_x\\ \varepsilon_y\\ \gamma_{xy}\end{Bmatrix}\ \text{and}\ \begin{Bmatrix}\tau_{yz}\\ \tau_{zx}\end{Bmatrix}=\begin{bmatrix}Q_{44}&0\\ 0&Q_{55}\end{bmatrix}\begin{Bmatrix}\gamma_{yz}\\ \gamma_{xz}\end{Bmatrix} \tag{11}$$

where $(\sigma_x, \sigma_y, \tau_{xy}, \tau_{yz}, \tau_{yx})$ and $(\varepsilon_x, \varepsilon_y, \gamma_{xy}, \gamma_{yz}, \gamma_{yx})$ are the stress and strain components, respectively. Using the material properties defined in Eq. (1), stiffness coefficients, Q_{ij}, can be expressed as:

$$Q_{11}=Q_{22}=\frac{E(z)}{1-\nu^2} \tag{12a}$$

$$Q_{12}=\frac{\nu E(z)}{1-\nu^2} \tag{12b}$$

$$Q_{44}=Q_{55}=Q_{66}=\frac{E(z)}{2(1+\nu)} \tag{12c}$$

Since the bottom surface of the plate is assumed subjected to Winkler–Pasternak elastic foundation (see Fig. 1), the reaction–deflection relation at the bottom surface of the model is expressed by:

$$f_e=k_0 w-k_1\nabla^2 w \tag{13}$$

where f_e is the density of reaction force of foundation. If the foundation is modeled as the linear Winkler foundation, the coefficient k_1 in Eq. (13) is zero.

2.2.3 Governing Equations

The governing equations of equilibrium can be derived by using the principle of virtual displacements. The principle of virtual work in the present case yields:

$$\int_{-h/2}^{h/2}\int_{\Omega}[\sigma_x\delta\varepsilon_x+\sigma_y\delta\varepsilon_y+\tau_{xy}\delta\gamma_{xy}+\tau_{yz}\delta\gamma_{yz}+\tau_{xz}\delta\gamma_{xz}]d\Omega dz+\int_{\Omega}[f_e\delta w]d\Omega$$
$$-\int_{\Omega}[q\delta w]d\Omega=0 \tag{14}$$

where Ω is the top surface.

Substituting Eqs. (8), (9) and (11) into Eq. (14) and integrating through the thickness of the plate, Eq. (14) can be rewritten as:

$$\int_{\Omega}[N_x\delta\varepsilon_x^0+N_y\delta\varepsilon_y^0+N_{xy}\delta\varepsilon_{xy}^0+M_x^b\delta k_x^b+M_y^b\delta k_y^b+M_{xy}^b\delta k_{xy}^b+M_x^s\delta k_x^s+M_y^s\delta k_y^s$$
$$+M_{xy}^s\delta k_{xy}^s+S_{yz}^s\delta\gamma_{yz}^s+S_{xz}^s\delta\gamma_{xz}^s]d\Omega+\int_{\Omega}f_e(\delta w_b+\delta w_s)d\Omega-\int_{\Omega}q(\delta w_b+\delta w_s)d\Omega$$
$$=0 \tag{15}$$

where

$$\begin{Bmatrix}N_x,&N_y,&N_{xy}\\ M_x^b,&M_y^b,&M_{xy}^b\\ M_x^s,&M_y^s,&M_{xy}^s\end{Bmatrix}=\int_{-h/2}^{h/2}(\sigma_x,\sigma_y,\tau_{xy})\begin{Bmatrix}1\\ z\\ f(z)\end{Bmatrix}dz \tag{16b}$$

$$(S_{xz}^s,S_{yz}^s)=\int_{-h/2}^{h/2}(\tau_{xz},\tau_{yz})g(z)dz \tag{16b}$$

The governing equations of equilibrium can be derived from Eq. (15) by integrating the displacement gradients by parts and setting the coefficients δu_0, δv_0, δw_b and δw_s zero separately. Thus one can obtain the equilibrium equations associated with the present shear deformation theory,

$$\delta u_0:\ \frac{\partial N_x}{\partial x}+\frac{\partial N_{xy}}{\partial y}=0$$

$$\delta v_0:\ \frac{\partial N_{xy}}{\partial x}+\frac{\partial N_y}{\partial y}=0$$

$$\delta w_b:\ \frac{\partial^2 M_x^b}{\partial x^2}+2\frac{\partial^2 M_{xy}^b}{\partial x\partial y}+\frac{\partial^2 M_y^b}{\partial y^2}-f_e+q=0$$

$$\delta w_s:\ \frac{\partial^2 M_x^s}{\partial x^2}+2\frac{\partial^2 M_{xy}^s}{\partial x\partial y}+\frac{\partial^2 M_y^s}{\partial y^2}+\frac{\partial^2 S_{xz}^s}{\partial x}+\frac{\partial^2 S_{yz}^s}{\partial y}-f_e+q=0 \tag{17}$$

Using Eq. (11) in Eq. (16), the stress resultants of a FGM plate can be related to the total strains by:

$$\begin{Bmatrix}N\\ M^b\\ M^s\end{Bmatrix}=\begin{bmatrix}A&B&B^s\\ A&D&D^s\\ B^s&D^s&H^s\end{bmatrix}\begin{Bmatrix}\varepsilon\\ k^b\\ k^s\end{Bmatrix},\ S=A^s\gamma \tag{18}$$

where

$$N=\{N_x,N_y,N_{xy}\}^t,\ M^b=\{M_x^b,M_y^b,M_{xy}^b\}^t,\ M^s=\{M_x^s,M_y^s,M_{xy}^s\}^t \tag{19a}$$

$$\varepsilon=\{\varepsilon_x^0,\varepsilon_y^0,\gamma_{xy}^0\}^t,\ k^b=\{k_x^b,k_y^b,k_{xy}^b\}^t,\ k^s=\{k_x^s,k_y^s,k_{xy}^s\}^t \tag{19b}$$

$$A=\begin{bmatrix}A_{11}&A_{12}&0\\ A_{12}&A_{22}&0\\ 0&0&A_{66}\end{bmatrix},\ B=\begin{bmatrix}B_{11}&B_{12}&0\\ B_{12}&B_{22}&0\\ 0&0&B_{66}\end{bmatrix},\ D=\begin{bmatrix}D_{11}&D_{12}&0\\ D_{12}&D_{22}&0\\ 0&0&D_{66}\end{bmatrix} \tag{19c}$$

$$B^s=\begin{bmatrix}B_{11}^s&B_{12}^s&0\\ B_{12}^s&B_{22}^s&0\\ 0&0&B_{66}^s\end{bmatrix},\ D^s=\begin{bmatrix}D_{11}^s&D_{12}^s&0\\ D_{12}^s&D_{22}^s&0\\ 0&0&D_{66}^s\end{bmatrix},\ H^s=\begin{bmatrix}H_{11}^s&H_{12}^s&0\\ H_{12}^s&H_{22}^s&0\\ 0&0&H_{66}^s\end{bmatrix} \tag{19d}$$

$$S=\{S_{xz}^s,S_{yz}^s\}^t,\ \gamma=\{\gamma_{xz},\gamma_{yz}\}^t,\ A^s=\begin{bmatrix}A_{44}^s&0\\ 0&A_{55}^s\end{bmatrix} \tag{19e}$$

where A_{ij}, B_{ij}, etc., are the plate stiffness, defined by

$$\begin{Bmatrix}A_{11}&B_{11}&D_{11}&B_{11}^s&D_{11}^s&H_{11}^s\\ A_{12}&B_{12}&D_{12}&B_{12}^s&D_{12}^s&H_{12}^s\\ A_{66}&B_{66}&D_{66}&B_{66}^s&D_{66}^s&H_{66}^s\end{Bmatrix}=\int_{-h/2}^{h/2}Q_{11}(1,z,z^2,f(z),zf(z),f^2(z))\begin{Bmatrix}1\\ \nu\\ \frac{1-\nu}{2}\end{Bmatrix}dz \tag{20a}$$

and

$$(A_{22},B_{22},D_{22},B_{22}^s,D_{22}^s,H_{22}^s)=(A_{11},B_{11},D_{11},B_{11}^s,D_{11}^s,H_{11}^s),\ Q_{11}=\frac{E(z)}{1-\nu^2} \tag{20b}$$

$$A_{44}^s = A_{55}^s = \int_{-h/2}^{h/2} \frac{E(z)}{2(1+\nu)}[g(z)]^2 dz \tag{20c}$$

Substituting from Eq. (18) into Eq. (17), we obtain the governing equations of equilibrium (given in the Appendix A).

2.3 Exact Solutions for FGM Plates

Rectangular plates are generally classified in accordance with the type support used. We are here concerned with the analytical solutions of equation (given in Appendix A) for simply supported FG plate. The following boundary conditions are imposed at the side edges.

$$v_0(0,y) = w_b(0,y) = w_s(0,y) = \frac{\partial w_s}{\partial y}(0,y) = 0 \tag{21a}$$

$$v_0(a,y) = w_b(a,y) = w_s(a,y) = \frac{\partial w_s}{\partial y}(a,y) = 0 \tag{21b}$$

$$N_x(0,y) = M_x^b(0,y) = M_x^s(0,y) = N_x(a,y) = M_x^b(a,y) = M_x^s(a,y) = 0 \tag{21c}$$

$$u_0(x,0) = w_b(x,0) = w_s(x,0) = \frac{\partial w_s}{\partial x}(x,0) = 0 \tag{21d}$$

$$u_0(x,b) = w_b(x,b) = w_s(x,b) = \frac{\partial w_s}{\partial x}(x,b) = 0 \tag{21e}$$

$$N_y(x,0) = M_y^b(x,0) = M_y^s(x,0) = N_y(x,b) = M_y^b(x,b) = M_y^s(x,b) = 0 \tag{21f}$$

To solve this problem, Navier presented the external force in the form of a double trigonometric series:

$$q(x,y) = \sum_{m=1}^{\infty}\sum_{n=1}^{\infty} q_{mn}\sin(\lambda x)\sin(\mu y) \tag{22}$$

where $\lambda = m\pi/a$ and $\mu = n\pi/b$, and m and n are mode numbers. For the case of a sinusoidally distributed load, we have

$$m = n = 1 \text{ , and } q_{11} = q_0 \tag{23}$$

where q_0 represents the intensity of the load at the plate center.

Following the Navier solution procedure, we assume the following solution form for (u_0, v_0, w_b, w_s) that satisfies the boundary conditions,

$$\begin{Bmatrix} u_0 \\ v_0 \\ w_b \\ w_s \end{Bmatrix} = \sum_{m=1}^{\infty}\sum_{n=1}^{\infty} \begin{bmatrix} U_{mn}\cos(\lambda x)\sin(\mu y) \\ V_{mn}\sin(\lambda x)\cos(\mu y) \\ W_{bmn}\sin(\lambda x)\sin(\mu y) \\ W_{smn}\sin(\lambda x)\sin(\mu y) \end{bmatrix} \tag{24}$$

where U_{mn}, V_{mn}, W_{mn}, W_{bmn}, and W_{smn} are arbitrary parameters to be determined.

Substituting Eqs. (24), (23) and (22) into equations of Appendix A we obtain:

$$[K]\{\Delta\} = \{F\} \tag{25}$$

where $\{\Delta\}$ and $\{F\}$ denotes the columns

$$\{\Delta\}^T = \{U_{mn}, V_{mn}, W_{bmn}, W_{smn}\} \text{ , and } \{F\}^T = \{0, 0, -q_{mn}, -q_{mn}\} \tag{26}$$

and

$$[K] = \begin{bmatrix} a_{11} & a_{12} & a_{13} & a_{14} \\ a_{12} & a_{22} & a_{23} & a_{24} \\ a_{13} & a_{23} & a_{33} & a_{34} \\ a_{14} & a_{24} & a_{34} & a_{44} \end{bmatrix} \tag{27}$$

The elements of the symmetric matrix [K] are defined in Appendix B.

3. Numerical Results

In this study, bending analysis of FG plates by the present new trigonometric shear deformation plate theory is suggested for investigation. The Poisson's ratio is fixed at $\nu = 0.3$. Comparisons are made with available solutions in literature. In order to verify the accuracy of the present analysis, some numerical examples are solved. The material properties used in the present study are:

- Metal (Aluminium, Al): $E_M = 70\times10^9$ N/m^2; $\nu = 0.3$.
- Ceramic (Alumina, Al_2O_3): $E_C = 380\times10^9$ N/m^2; $\nu = 0.3$.

The various non-dimensional parameters used are

$$\bar{w} = \frac{10h^3E_c}{a^4q_0}w\left(\frac{a}{2},\frac{b}{2}\right),\ \bar{\sigma}_x = \frac{h}{aq_0}\sigma_x\left(\frac{a}{2},\frac{b}{2},\frac{h}{2}\right),\ \bar{\tau}_{xy} = \frac{h}{aq_0}\tau_{xy}\left(0,0,-\frac{h}{3}\right)$$

$$\bar{\tau}_{xz} = \frac{h}{aq_0}\tau_{xz}\left(0,\frac{b}{2},0\right),\ \bar{z} = z/h,\ K_0 = k_0a^4/D,\ K_1 = k_1a^2/D$$

where $D = Eh^3/12(1-\nu^2)$ is a reference bending rigidity of the plate.

Table 1 gives the effects of side-to-thickness ratio and elastic foundation parameters on the dimensionless center deflection and stresses of anisotropic square plate. It is clear that the center deflection $\bar{w}$, and the axial stress $\bar{\sigma}_x$ decrease as the side-to-thickness ratio a/h increases. However, the shear stresses ($\bar{\tau}_{xy}$ and $\bar{\tau}_{xz}$) increase as the side-to-thickness ratio a/h increases. In addition, both the center deflection and stresses are decreasing with the existence of the elastic foundations. The inclusion of the Winkler foundation parameter gives results more than those with the inclusion of Pasternak foundation parameters. As observed in Table 1, there is a very good agreement between the present new trigonometric shear deformation plate theory and other higher-order plate theories. The FSDPT results are upper bounds of present theory and HPT solutions while the CPT results are lower bounds of them and it is independent, as it is well known, of the side-to-thickness ratio.

In Table 2, the effects of volume fraction exponent and the foundation parameters on the dimensionless stresses and the center deflection of homogeneous and FGM plates are given. It is seen from the presented results in Table 2 that, decrement occurs for shear stresses ($\bar{\tau}_{xy}$ and $\bar{\tau}_{xz}$) and the axial stress $\bar{\sigma}_x$, together with the center deflection $\bar{w}$ of the plate as either K_0 or K_1 increases. It is indicated that large moduli of elastic foundation can enhance bending rigidity of the plate. The stresses and deflection of the plate are greatly influenced by graded index p, which means that the plate can be optimally design according to given working conditions by tailoring the graded material

Table 1. Effects of Side-to-thickness Ratio and Elastic Foundation Parameters on the Dimensionless Deflection and Stresses of an Isotropic Square FGM Plate

a/h	K_0	K_1	Theory	$\bar{w}$	$\bar{\sigma}_x$	$\bar{\tau}_{xy}$	$\bar{\tau}_{xz}$
5	0	0	ESDPT	0.3428578	1.029440	0.3489582	0.2530360
			SSDPT	0.3431864	1.027258	0.3491764	0.2455716
			PSDPT	0.3433163	1.024924	0.3494526	0.2380930
			FSDPT	0.3434858	0.9878816	0.3546240	0.1909859
			CPT	0.2802613	0.9878810	0.3546238	-
			Present	0.3431864	1.027258	0.3491766	0.2455716
	100	0	ESDPT	0.2609323	0.7834560	0.2655750	0.1925733
			SSDPT	0.2611226	0.7816170	0.2656804	0.1868497
			PSDPT	0.2611978	0.7797708	0.2658662	0.1811430
			FSDPT	0.2612958	0.7514992	0.2697690	0.1452864
			CPT	0.2230227	0.7861232	0.2821980	-
			Present	0.2611226	0.7816172	0.2656804	0.1868497
	0	10	ESDPT	0.2116725	0.6355520	0.2154386	0.1562185
			SSDPT	0.2117976	0.6339732	0.2154946	0.1515546
			PSDPT	0.2118472	0.6324408	0.2156338	0.1469178
			FSDPT	0.2119115	0.6094678	0.2187832	0.1178277
			CPT	0.1860216	0.6556996	0.2353796	-
			Present	0.2117976	0.6339728	0.2154944	0.1515546
	100	10	ESDPT	0.1773040	0.5323598	0.1804586	0.1308539
			SSDPT	0.1773918	0.5309862	0.1804880	0.1269350
			PSDPT	0.1774266	0.5296830	0.1805977	0.1230469
			FSDPT	0.1774717	0.5104170	0.1832266	0.09867832
			CPT	0.1589454	0.5602600	0.2011190	-
			Present	0.1773918	0.5309862	0.1804881	0.1269350
10	100	10	ESDPT	0.1638744	1.105538	0.3911440	0.1405294
			SSDPT	0.1638971	1.104803	0.3911620	0.1362969
			PSDPT	0.1639048	1.104109	0.3912240	0.1320798
			FSDPT	0.1639081	1.093818	0.3926523	0.1057331
			CPT	0.1589454	1.120520	0.4022380	-
			Present	0.1638971	1.104804	0.3911616	0.1362969
20	100	10	ESDPT	0.1602009	2.233407	0.7988240	0.1431760
			SSDPT	0.1602066	2.233034	0.7988335	0.1388572
			TSDPT	0.1602084	2.232680	0.7988655	0.1345492
			FSDPT	0.1602086	2.227444	0.7995950	0.1076574
			CPT	0.1589454	2.241039	0.8044750	-
			Present	0.1602066	2.233034	0.7988330	0.1388572
50	100	10	ESDPT	0.1591473	5.599530	2.008916	0.1439351
			SSDPT	0.1591483	5.599378	2.008920	0.1395914
			PSDPT	0.1591486	5.599238	2.008934	0.1352572
			FSDPT	0.1591486	5.597134	2.009226	0.1082087
			CPT	0.1589454	5.602600	2.011190	-
			Present	0.1591483	5.599376	2.008920	0.1395914
100	100	10	ESDPT	0.1589959	11.20366	4.021240	0.1440442
			SSDPT	0.1589961	11.20359	4.021243	0.1396969
			PSDPT	0.1589962	11.20353	4.021248	0.1353590
			FSDPT	0.1589962	11.20247	4.021396	0.1082879
			CPT	0.1589454	11.20520	4.022380	-
			Present	0.1589961	11.20359	4.021242	0.1396969

Table 2. Effects of Volume Fraction Exponent and Elastic Foundation Parameters on the Dimensionless Displacements and Stresses of a FGM Square Plate According to Present Method (a/h = 10)

p	K_0	K_0	$\bar{w}$	$\bar{\sigma}_x$	$\bar{\tau}_{xy}$	$\bar{\tau}_{xz}$
ceramic	0	0	0.2960316	1.995501	0.7065175	0.2461800
	100	0	0.2328956	1.569911	0.5558353	0.1936761
	0	10	0.1928403	1.299905	0.4602384	0.1603661
	100	10	0.1638971	1.104804	0.3911616	0.1362969
1	0	0	0.5889103	3.086997	0.6110370	0.2461801
	100	0	0.3825844	2.005461	0.3969590	0.1599303
	0	10	0.2852521	1.495256	0.2959696	0.1192429
	100	10	0.2261716	1.185564	0.2346694	0.09454569
2	0	0	0.7573320	3.609363	0.5440948	0.2265014
	100	0	0.4471920	2.131269	0.3212792	0.1337453
	0	10	0.3196886	1.523601	0.2296758	0.09561179
	100	10	0.2472924	1.178569	0.1776638	0.07395969
5	0	0	0.9118358	4.248830	0.5754613	0.2016656
	100	0	0.4969093	2.315417	0.3136003	0.1098986
	0	10	0.3443160	1.604390	0.2172985	0.07615042
	100	10	0.2617760	1.219782	0.1652073	0.05789552
10	0	0	1.008921	5.089009	0.5893748	0.2198098
	100	0	0.5244087	2.645125	0.3063405	0.1142511
	0	10	0.3572988	1.802220	0.2087210	0.07784337
	100	10	0.2692131	1.357914	0.1572645	0.05865248
metal	0	0	1.607028	1.995501	0.7065178	0.2461801
	100	0	0.6501876	0.8073596	0.2858501	0.09960199
	0	10	0.4115419	0.5110251	0.1809312	0.06304397
	100	10	0.2988967	0.3711501	0.1314078	0.04578789

properties. In fact, it is found that the deflection increases as volume fraction index p increases. This is due to the fact that the bending stiffness is the maximum for fully ceramic plate, i.e., (p = 0) and degrades gradually as n increases. It is important to observe that the stresses for a fully ceramic plate are the same as that for a fully metal plate without elastic foundations ($K_0 = K_1 =$ 0). This is because the plate for these two cases is fully homogeneous and the stresses do not depend on the modulus of elasticity. This observation may be slightly changed with the inclusion of the foundation parameters that always underpredict the magnitude of the center deflection and stresses.

Figure 3 shows the variation of the center deflection $\bar{w}$ with the side-to-thickness a/h. The deflection is maximum for the metallic plate and minimum for the ceramic plate. It decreases with the increase of a/h ratios. The difference is almost constant with the increase of side-to-thickness ratio. One of the main inferences from the analysis is that the response of FGM plates is intermediate to those of the ceramic and metal homogeneous plates (see also Table 2).

Figures 4-5 depict the through-the-thickness distributions of the axial stress $\bar{\sigma}_x$ in the FGM (p = 2) square plates under the sinusoidal loads. As exhibited in Figs. 4 and 5, the axial stress $\bar{\sigma}_x$, is compressive throughout the plate up to $\bar{z}$ = 0.153 and then they become tensile. The maximum compressive stresses occur

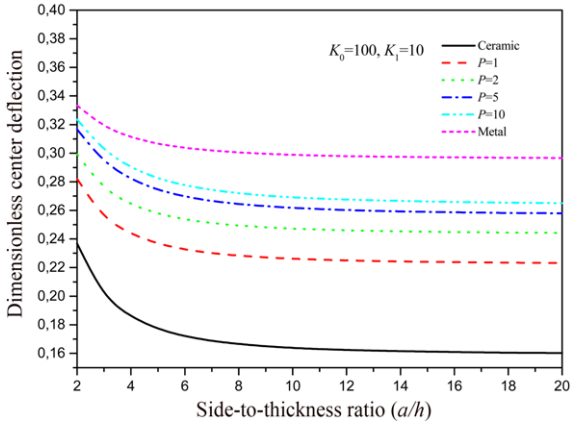

Fig. 3. Dimensionless Center Deflection $\bar{w}$ versus Side-to-thickness Ratio a/h for FGM Square Plate on Elastic Foundations

at a point on the bottom surface and the maximum tensile stresses occur, of course, at a point on the top surface of the FGM plate. In addition, it can be seen from these figures that the elastic foundation has a significant effect on the maximum values of the axial stress $\bar{\sigma}_x$. It is observed that normal stress ($\bar{\sigma}_x$) increases gradually with decreasing K_0 or K_1.

Figures 6-7 depict the through-the-thickness distributions of

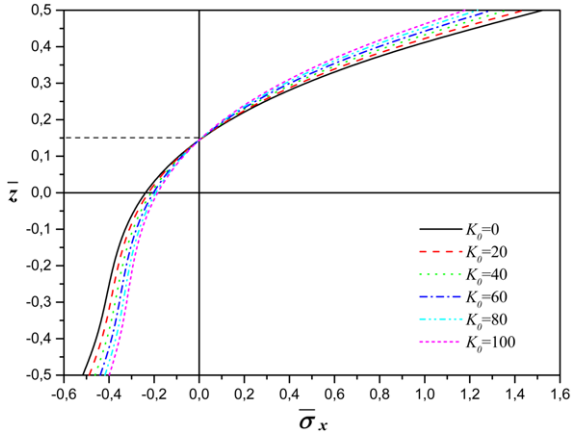

Fig. 4. Variation of In-plane Longitudinal Stress ($\bar{\sigma}_x$) Through-the-thickness of a Square FGM Plate for Different Values of K_0 (a/h = 10, p = 2 and K_1 =10)

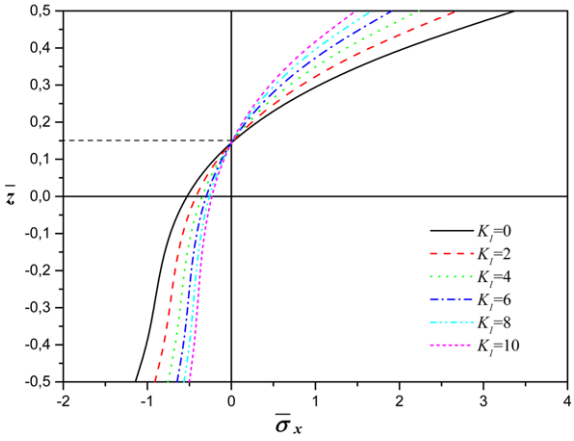

Fig. 5. Variation of the Axial Stress ($\bar{\sigma}_x$) Through-the-thickness of a Square FGM Plate for Different Values of K_1 (a/h = 10, p = 2 and K_0 =10)

the shear stresses $\bar{\tau}_{xz}$ in the square FGM plate under sinusoidal distributed load. The volume fraction exponent of the FGM plate is taken as $p = 2$ in these figures. Distinction between the curves in Figs. 6 and 7 is obvious. It is observed that transverse shear stress ($\bar{\tau}_{xz}$) increases gradually with decreasing K_0 or K_1. It is indicated that large moduli of elastic foundation can enhance bending rigidity of the plate. The through-the-thickness distributions of the shear stress $\bar{\tau}_{xz}$ are not parabolic as in the plate made of pure material. It is to be noted that the maximum value occurs at $z \cong 0.2$, not at the plate center as in the homogeneous case.

Figures 8-9 show the longitudinal tangential stress $\bar{\tau}_{xy}$ in the FGM ($p = 2$) square plates under the sinusoidal loads. Contrary to the axial stress, the tensile and compressive values of the longitudinal tangential stress, $\bar{\tau}_{xy}$ (Figs. 8 and 9), is maximum at a point on the bottom and top surfaces of the FGM plate, respectively. It is clear that the minimum value of zero for all axial stresses $\bar{\sigma}_x$ and $\bar{\tau}_{xy}$ occurs at $z = 0.153$.

Finally, the exact maximum deflections of simply supported FGM square plate are compared in Figs. 10 and 11 for various

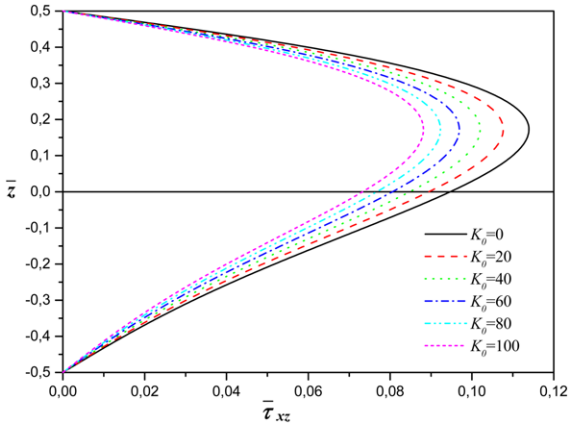

Fig. 6. Variation of Transversal Shear Stress ($\bar{\tau}_{xz}$) Through-the-thickness of a Square FGM Plate for Different Values of K_0 (a/h = 10, p = 2 and K_1 =10)

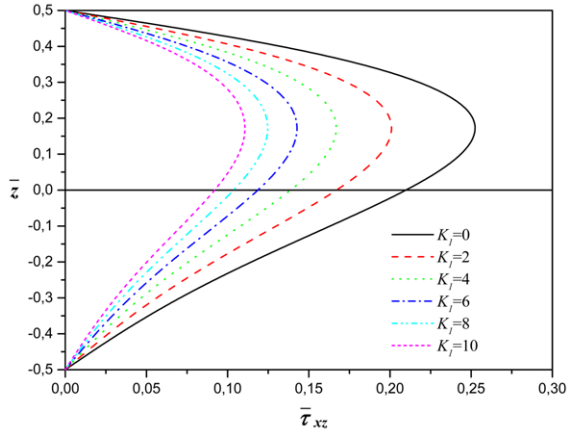

Fig. 7. Variation of Transversal Shear Stress ($\bar{\tau}_{xz}$) Through-the-thickness of a Square FGM Plate for Different Values of K_1 (a/h = 10, p = 2 and K_0 =10)

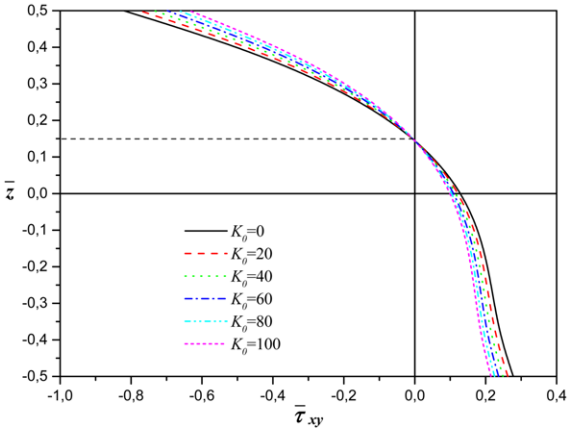

Fig. 8. Variation of Longitudinal Stress ($\bar{\tau}_{xz}$) Through-the-thickness of a Square FGM Plate for Different Values of K_0 (a/h = 10, p = 2 and K_1 =10)

ratios of moduli, E_m/E_c. This means that the deflections are computed for plates with different ceramic–metal mixtures. It is

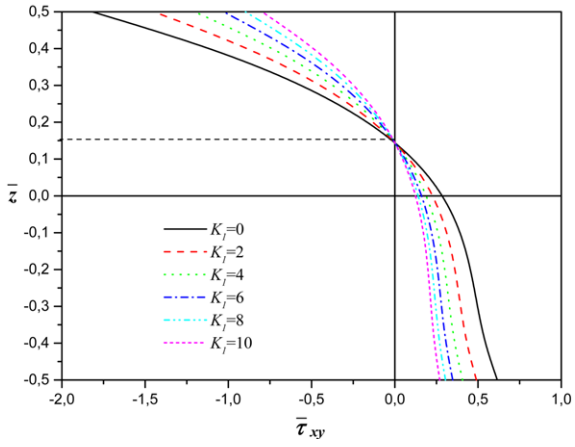

Fig. 9. Variation of Longitudinal Tangential Stress ($\bar{\tau}_{xz}$) Through-the-thickness of a square FGM plate for different values of K_1 (a/h = 10, p = 2 and K_0 =10)

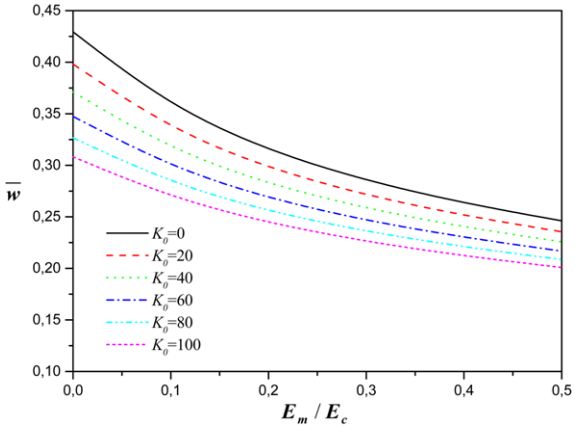

Fig. 10. The effect of material anisotropy on the dimensionless maximum deflection ($\bar{w}$) of a square FGM plate for different values of K_0 (a/h = 10, p = 2 and K_1 =10)

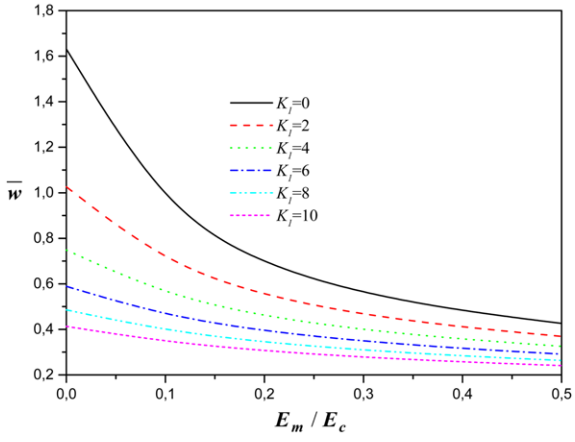

Fig. 11. The Effect of Material Anisotropy on the Dimensionless Maximum Deflection ($\bar{w}$) of a Square FGM Plate for Different Values of K_1 (a/h = 10, p = 2 and K_0 =10)

clear that the deflections decrease smoothly as the ratio of metal-to-ceramic moduli increases. Further, the deflections decrease gradually as either K_0 or K_1 increases.

4. Conclusions

The bending response of functionally graded plates resting on a Winkler-Pasternak elastic foundation is studied using a new trigonometric shear deformation theory. The number of primary variables in this theory is even less than that of first- and higher-order shear deformation plate theories. The theory gives parabolic distribution of transverse shear strains, and satisfies the zero traction boundary conditions on the surfaces of the plate without using shear correction factors. The stress and displacement response of the plates have been analyzed under sinusoidal loading. The gradation of properties through the thickness is assumed to be of the power law type and comparisons have been made with homogeneous isotropic plates. Non-dimensional stresses and displacements are computed for plates with ceramic-metal mixture. It is seen that the basic response of the plates that correspond to properties intermediate to that of the metal and ceramic, is necessarily lie in between that of ceramic and metal. This behaviour is found to be true irrespective of boundary conditions. Thus, the gradients in material properties play an important role in determining the response of the FGM plates. It can be seen from the results that deflections and the stresses decrease gradually as either K_0 or K_1 increases. Numerical results given in the present paper render a benchmark for the analyses of FGM thick plates on elastic foundations in the future.

References

Ait Atmane, H., Tounsi, A., Mechab, I., and Adda Bedia, E. A. (2010). "Free vibration analysis of functionally graded plates resting on Winkler-Pasternak elastic foundations using a new shear deformation theory." *Int. J. Mech. Mater. Des*, Vol. 6, No. 2, pp. 113-121.

Chehel Amirani, M., Khalili, S. M. R., and Nemati, N. (2009). "Free vibration analysis of sandwich beam with FG core using the element free Galerkin method." *Composite. Structures*, Vol. 90, pp. 373-379.

Cheng, Z. Q. and Batra, B. C. (2000). "Exact correspondence between eigenvalues of membranes and functionally graded simply supported polygonal plate." *J. Sound. Vib*, Vol. 229, No. 4, pp. 879-895.

Cheng, Z. Q. and Kitipornchai, S. (1999). "Membrane analogy of buckling and vibration of inhomogeneous plates." *ASCE. J. Eng. Mech*, Vol. 125, No. 11, pp. 1293-1297.

Hill, R. (1965). "A self-consistent mechanics of composite materials." *J. Mech. Phys. Solids*, Vol. 13, pp. 213-222.

Karama, M., Afaq, K. S., and Mistou, S. (2003). "Mechanical behaviour of laminated composite beam by new multi-layered laminated composite structures model with transverse shear stress continuity." *Int. J. Solids. Struct*, Vol. 40, No. 6, pp. 1525-1546.

Koizumi, M. (1993). "The concept of FGM. Ceramic transactions." functionally gradient materials, Vol. 34, No. 1, pp. 3-10.

Koizumi, M. (1997). "FGM activities in Japan." *Compos. Part. B: Eng*, Vol. 28, p. 1-4.

Mechab, I., Ait Atmane, H., Tounsi, A., Belhadj, H., and Adda bedia, E. A. (2010). "A two variable refined plate theory for bending of functionally graded plates." *Acta. Mech. Sin*, Vol. 26, No. 6, pp. 941.

Mori, T. and Tanaka, K. (1973). "Average stress in matrix and average

elastic energy of materials with misfitting inclusions." *Acta. Metall,* Vol. 21, pp. 571-574.

Pasternak, P. L. (1954). *On a new method of analysis of an elastic foundation by means of two foundation constants,* Gosudarstvennoe Izdatelstvo Literaturi po Stroitelstvu I Arkhitekture, Moscow, USSR, Vol. 1, pp. 1-56 (in Russian).

Praveen, G. N. and Reddy, J. N. (1998). "Nonlinear transient thermoelastic analysis of functionally graded ceramic–metal plates." *Int. J. Solids Struct*, Vol. 35, pp. 4457-4476.

Reddy, J. N. (1984). "A simple higher order theory for laminated composite plates." *J. Appl. Mech,* Vol. 51, pp. 745-752.

Reddy, J. N. and Cheng, Z. Q. (2002). "Frequency correspondence between membranes and functionally graded spherical shallow shells of polygonal planform." *Int. J. Mech. Sci*, Vol. 44, No. 5, pp. 967-985.

Suresh, S. and Mortensen, A. (1998). *Fundamentals of functionally graded materials*, London: IOM Communications.

Suresh, S. and Mortensen, A. (1997). "Functionally graded metals and metal-ceramic composites 2: thermomechanical behaviour." *Int. Mater. Rev*, Vol. 42, No. 3, pp. 85-116.

Tanigawa, Y. (1995). "Some basic thermoelastic problems for nonhomogeneous structural materials." *Appl. Mech. Rev*, Vol. 48, No. 6, pp. 287-300.

Touratier, M. (1991). "An efficient standard plate theory." *Int. J. Eng. Sci*, Vol. 29, No. 8, pp. 901-916.

Winkler, E. (1867). *Die Lehre von der Elasticitaet und Festigkeit*, Prag Dominicus.

Appendix A

The governing equations of equilibrium are as follows:

$$A_{11}\frac{\partial^2 u_0}{\partial x^2}+A_{66}\frac{\partial^2 u_0}{\partial y^2}+(A_{12}+A_{66})\frac{\partial^2 v_0}{\partial x\partial y}-B_{11}\frac{\partial^3 w_b}{\partial x^3}-(B_{12}+2B_{66})\frac{\partial^3 w_s}{\partial x\partial y^2}-B^s_{11}\frac{\partial^3 w_s}{\partial x^3}$$
$$-(B^s_{12}+2B^s_{66})\frac{\partial^3 w_s}{\partial x\partial y^2}=0 \tag{A.1}$$

$$(A_{12}+A_{66})\frac{\partial^2 u_0}{\partial x\partial y}+A_{66}\frac{\partial^2 v_0}{\partial x^2}+A_{22}\frac{\partial^2 v_0}{\partial y^2}-(B_{12}+2B_{66})\frac{\partial^3 w_b}{\partial x^2\partial y}-B_{22}\frac{\partial^3 w_b}{\partial y^3}$$
$$-(B^s_{12}+2B^s_{66})\frac{\partial^3 w_s}{\partial x^2\partial y}-B^s_{22}\frac{\partial^3 w_s}{\partial y^3}=0 \tag{A.2}$$

$$B_{11}\frac{\partial^3 u_0}{\partial x^3}+(B_{12}+2B_{66})\frac{\partial^3 u_0}{\partial x\partial y^2}+(B_{12}+2B_{66})\frac{\partial^3 v_0}{\partial x^2\partial y}+B_{22}\frac{\partial^3 v_0}{\partial y^3}-D_{11}\frac{\partial^4 w_b}{\partial x^4}$$
$$-2(D_{12}+2D_{66})\frac{\partial^4 w_b}{\partial x^2\partial y^2}-D_{22}\frac{\partial^4 w_b}{\partial y^4}-D^s_{11}\frac{\partial^4 w_s}{\partial x^4}-2(D^s_{12}+2D^s_{66})\frac{\partial^4 w_s}{\partial x^2\partial y^2}-D^s_{22}\frac{\partial^4 w_s}{\partial y^4}$$
$$-f_e+q=0 \tag{A3}$$

$$B^s_{11}\frac{\partial^3 u_0}{\partial x^3}+(B^s_{12}+2B^s_{66})\frac{\partial^3 u_0}{\partial x\partial y^2}+(B^s_{12}+B^s_{66})\frac{\partial^3 v_0}{\partial x^2\partial y}+B^s_{22}\frac{\partial^3 v_0}{\partial y^3}-D^s_{11}\frac{\partial^4 w_b}{\partial x^4}$$
$$-2(D^s_{12}+2D^s_{66})\frac{\partial^4 w_b}{\partial x^2\partial y^2}-D^s_{22}\frac{\partial^4 w_b}{\partial y^4}-H^s_{11}\frac{\partial^4 w_s}{\partial x^4}-2(H^s_{12}+2H^s_{66})\frac{\partial^4 w_s}{\partial x^2\partial y^2}$$
$$-H^s_{22}\frac{\partial^4 w_s}{\partial x^2}+A^s_{55}\frac{\partial^2 w_s}{\partial x^2}+A^s_{44}\frac{\partial^2 w_s}{\partial y^2}-f_e+q=0 \tag{A4}$$

Appendix B

The elements $a_{ij}=a_{ji}$ of the coefficient matrix $[K]$ in Eq. (27) are given by:

$$\begin{aligned}
a_{11}&=-(A_{11}\lambda^2+A_{66}\mu^2)\\
a_{12}&=-\lambda\mu(A_{12}+A_{66})\\
a_{13}&=\lambda[B_{11}\lambda^2+(B_{12}+2B_{66})\mu^2]\\
a_{14}&=-\lambda[B^s_{11}\lambda^2+(B^s_{12}+2B^s_{66})\mu^2]\\
a_{22}&=-(A_{66}\lambda^2+A_{22}\mu^2)\\
a_{23}&=\mu[(B_{12}+2B_{66})\lambda^2+B_{22}\mu^2]\\
a_{24}&=-\mu[(B^s_{12}+2B^s_{66})\lambda^2+B^s_{22}\mu^2]\\
a_{33}&=-(D_{11}\lambda^4+2(D_{12}+2D_{66})\lambda^2\mu^2+D_{22}\mu^4+k_1(\lambda^2+\mu^2)+k_0)\\
a_{34}&=(D^s_{11}\lambda^4+2(D^s_{12}+2D^s_{66})\lambda^2\mu^2+D^s_{22}\mu^4-k_1(\lambda^2+\mu^2)-k_0)\\
a_{44}&=-\begin{pmatrix}H^s_{11}\lambda^4+2(H^s_{12}+2H^s_{66})\lambda^2\mu^2+H^s_{22}\mu^4+A^s_{55}\lambda^2+A^s_{44}\mu^2\\+k_1(\lambda^2+\mu^2)+k_0\end{pmatrix}
\end{aligned} \tag{B}$$